Robust shadow-mask evaporation via lithographically controlled undercut

B. Cord,[a] C. Dames, and K. K. Berggren
Massachusetts Institute of Technology, Cambridge, Massachusetts 02139-4309

J. Aumentado
National Institute of Standards and Technology, Boulder, Colorado 80305

(Received 6 February 2006; accepted 4 September 2006; published 4 December 2006)

Suspended shadow-mask evaporation is a simple, robust technique for fabricating Josephson-junction structures using scanning electron-beam lithography. The basic process entails the fabrication of an undercut structure in a resist bilayer to form a suspended "bridge," followed by two angle evaporations of superconducting material with a brief oxidation step in between. The result is two overlapping wires separated by a thin layer of oxide. Josephson junctions with sub-50-nm diameters are of particular interest in quantum computing research. Unfortunately, standard shadow-mask fabrication techniques are highly variable at linewidths below 100 nm, due to the difficulty of simultaneously fabricating a narrow line and a large undercut region. While most previous processes used poly(methylmethacrylate) (PMMA) for the top (imaging)layer and either lower-molecular-weight PMMA or a PMMA/methacrylic acid copolymer for the bottom (support) layer, the authors' process uses a PMMA/poly(methylglutarimide) (PMGI) bilayer. The advantage of using PMGI as the support layer is that it develops in aqueous base solutions, while PMMA is insensitive to aqueous solutions and only develops in certain organic solvents. This allows the two layers to be developed independently, ensuring that the imaging layer is not biased during the development of the support layer and allowing the process to achieve the full resolution of the PMMA imaging layer, which can be extremely high. Additionally, the extent of the undercut in the support layer can be precisely controlled by defining it lithographically, rather than simply varying the PMGI development time as in previous processes. Although PMGI is sold as a "liftoff resist" and widely assumed to be electron insensitive, their experiments have shown that this is not the case. Instead, when dilute developer and low electron doses are used, PMGI behaves very much like a conventional photoresist. By exploiting this behavior, as well as its high electron sensitivity with respect to PMMA, the authors were able to define undercuts by defining low-dose regions adjacent to their features, exposing the underlying PMGI separately. In this manner, it is possible to create well-controlled undercut regions as large as 600 nm. Extensive modeling of both the exposure and development processes was used to verify their results. By using a Monte Carlo simulation of electron scattering to simulate the electron exposure and mass-transfer relationships to simulate the process of developing the undercut region, the authors were able to produce a model that closely matches experimental results. With the process fully characterized, it is possible to produce nearly any linewidth/undercut combination, limited only by PMMA resolution and the mechanical stability of large overhang structures. This robustness, combined with the high resolution of the PMMA imaging layer, will allow the reliable fabrication of many interesting devices and circuits based on nanoscale Josephson junctions. © *2006 American Vacuum Society.* [DOI: 10.1116/1.2375090]

I. INTRODUCTION

Suspended shadow-mask evaporation is a simple, robust technique for fabricating Josephson-junction structures.[1] In the basic suspended shadow-mask process illustrated in Fig. 1, scanning electron-beam lithography (SEBL) is used to form an undercut structure in a photoresist bilayer to form a suspended "bridge" of resist between two open features. Superconducting material is then evaporated at an angle into the suspended region. The evaporated metal is then oxidized, and a second layer of metal is evaporated on top of it from the opposite angle. The resist is removed using solvents, and the remaining structure consists of two overlapping wires with a thin oxide barrier between them. Josephson junctions are of particular interest to the quantum computing field, and there has been recent interest in fabricating junctions with sub-50-nm diameters.[2] With its low processing overhead and compatibility with SEBL, suspended shadow-mask evaporation would seem to be an ideal candidate for sub-50-nm Josephson-junction fabrication.

Unfortunately, traditional shadow-mask processes have suffered from a lack of robustness at dimensions below 75 nm, with significant run-to-run variability and poor process control. Current shadow-mask processes typically use a resist bilayer consisting of a thin poly(methylmethacrylate) (PMMA) imaging layer on top of a thicker support layer of low-molecular-weight PMMA or PMMA/methacrylic acid copolymer, relying on the difference in sensitivity between

[a]Electronic mail: bcord@mit.edu

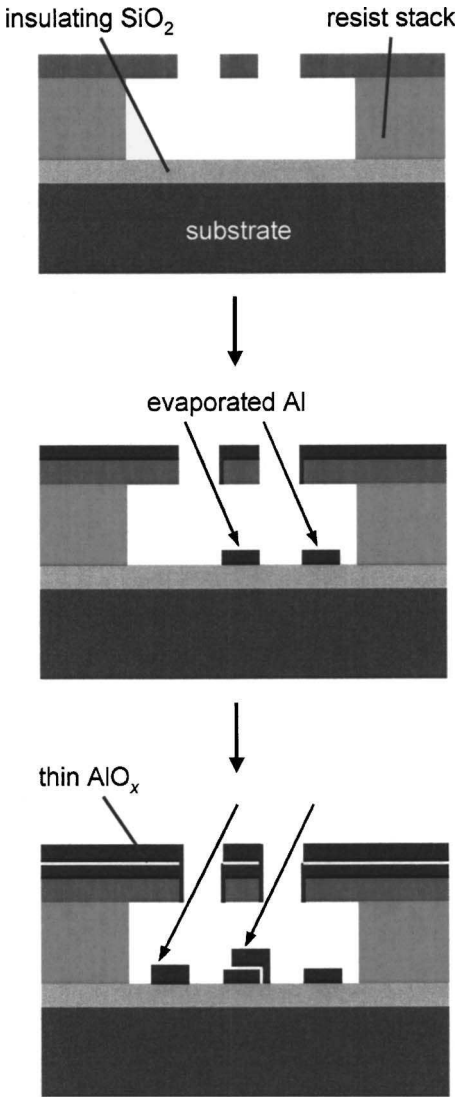

FIG. 1. Schematic cross-sectional diagram of the shadow-mask evaporation process, showing a general bilayer resist structure and double-angle evaporation needed to produce a Josephson junction.

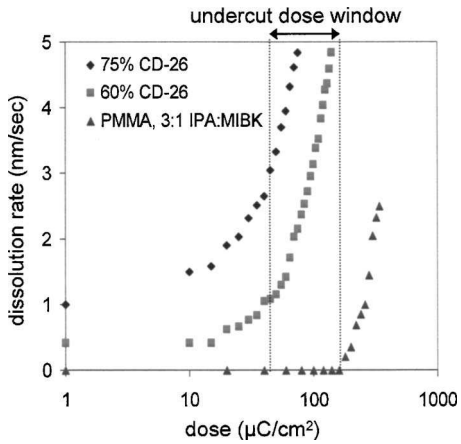

FIG. 2. Contrast curve plots for PMGI using two different dilutions of CD-26 developer. Contrast data for PMMA, developed using 3:1 IPA:MIBK, is shown for reference (development time for all samples was 60 s). The sensitivity difference between PMGI and PMMA is the dose range in which the PMGI can be exposed without affecting the PMMA, indicated by the two vertical lines in the figure.

the two resists to produce suitable undercut.[3] However, the long development time needed to create large undercut regions in the support layer can cause significant biasing of the imaging layer features, degrading process resolution. While this effect is a negligible issue for larger shadow-mask structures, reliably fabricating sub-75-nm features with this process is problematic.

The biasing problem can be mitigated by using poly(methylglutarimide) (PMGI) as the support layer.[4] PMGI is not affected by the organic solvents used to develop PMMA, instead developing in aqueous base solutions, which in turn have no effect on PMMA. As a result, the two layers can be developed independently, ensuring that the features in the imaging layer are not enlarged during the development of the undercut structure. In addition, PMGI is a "liftoff resist," meaning that it dissolves in developer without being exposed to radiation or electrons. In principle, developing the PMMA imaging layer, then varying the PMGI layer development time should allow the extent of the undercut to be accurately controlled. In practice, however, small variations in factors such as temperature, developer concentration, and feature size can cause significant run-to-run variations in the undercut. Since an undercut that is too small will complicate the liftoff process and an undercut that is too large will collapse the imaging layer, the PMMA/PMGI process suffers from a lack of robustness, despite its improved resolution.

By using a PMMA/PMGI bilayer and using SEBL to control the undercut, we have developed a high-resolution shadow-mask evaporation process that is much more robust than previous methods. The resulting lithographically defined undercuts are largely independent of PMGI development time and conditions, making it possible to reproducibly define arbitrary undercuts larger than 500 nm. Combined with the high resolution of the PMMA imaging layer, the process allows the fabrication of nanoscale Josephson-junction structures without the repeatability problems present in other PMGI-based processes.

II. PROCESS CHARACTERIZATION AND EXPOSURE MODEL

While PMGI is widely assumed to be insensitive to electron exposure, our experimental characterization of the material has shown that this is not the case. Instead, when low electron doses and dilute developer are used, PMGI exhibits contrast behavior very similar to that of a conventional electron-beam resist (Fig. 2). While it still dissolves in alkaline developers without being exposed, even low doses of electrons can increase the dissolution rate of PMGI by as much as a factor of 10. This behavior, coupled with PMGI's high electron sensitivity with respect to PMMA, allows PMGI in a bilayer to be selectively exposed by using electron doses low enough to pass through the PMMA imaging

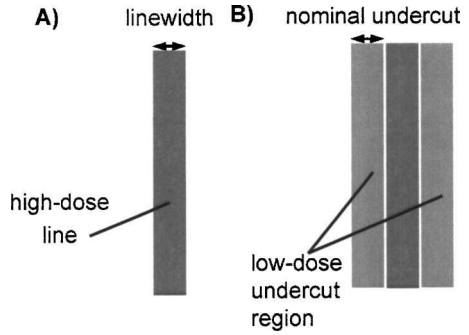

FIG. 3. Schematic overhead-view diagram of a method for defining an undercut region during electron-beam lithography. A high-dose feature is first exposed in the PMMA (A), followed by a low-dose exposure on either side of the line to define the undercut (B). If the undercut dose falls within the exposure window shown in Fig. 2, the support layer should be exposed without affecting the imaging layer. The two regions are separated by 1–2 pixels to avoid further dosing of the line while writing the undercut.

layer without affecting it, allowing low-dose undercut regions to be defined next to features during SEBL exposure (Fig. 3).

In order to formulate a complete model of the exposure process, the scattering properties of the PMMA/PMGI were examined in addition to its contrast behavior. A Monte Carlo model was used to simulate the bombardment of a typical bilayer with 30 keV electrons using CASINO, a free program for modeling electron scattering behavior in materials.[5] The simulation results, a three-dimensional plot of deposited energy density versus position in the bilayer, were integrated along one lateral dimension to obtain a two-dimensional data set, then plotted as one-dimensional representations of the electron point-spread function at various depths. The point-spread function plots were then fitted to the standard double-Gaussian model used to model electron scattering in materials:[6]

$$E(r) = \frac{D_n}{\pi}\left(\frac{1}{\alpha^2}e^{-(r^2/\alpha^2)} + \frac{\eta}{\beta^2}e^{-(r^2/\beta^2)}\right), \quad (1)$$

where E is the actual dose at a given point, D_n is the nominal electron dose, α is the forward-scattering parameter, β is the backscattering parameter, η is the ratio of backscattered electrons to incident electrons, and r is the radial distance from the center of the function. The double-Gaussian model allows the entire Monte Carlo data set to be reduced to a table expressing the three scattering parameters as a function of resist depth (Table I). In order to verify the Monte Carlo results, the point-spread function was measured experimentally[7] and the backscattering coefficient β was shown to be within 10% of the surface β in the model (Fig. 4).

Using the scattering data obtained from the Monte Carlo simulation and the experimental resist-contrast data, it is possible to simulate the exposure of a PMMA/PMGI bilayer and create a predictive model of the two-dose process outlined in Fig. 2. In order to do this, a feature with a given PMMA linewidth and PMGI undercut dimension was convolved with the point-spread functions at several resist depths. The resulting dose profile was then combined with the contrast curve data for each resist type, giving two-dimensional cross sections of the resist profile showing contours of constant development rate. As expected, the additional dosing of the PMGI adjacent to the feature increased its dissolution rate by nearly a factor of 5, indicating that lithographic control of the undercut was a viable alternative to development-based undercut processes.

TABLE I. Double-Gaussian scattering parameters as a function of depth for a resist bilayer consisting of 100 nm PMMA on 250 nm PMGI, based on data from Monte Carlo simulations. The top-layer η value is a spurious result thought to be caused by a mesh-boundary problem in the software.

Depth (nm)	Material	α (nm)	β (nm)	η
50	PMMA	5.20	4090	*3.2*
100	PMMA	4.87	3650	0.42
150	PMGI	6.40	3770	0.68
200	PMGI	7.23	3710	0.74
250	PMGI	8.46	3420	0.82
300	PMGI	9.84	3280	0.94
350	PMGI	12.75	2970	0.95

III. EXPERIMENTAL RESULTS

Modeling of the PMMA/PMGI-bilayer exposure process indicated that it should be possible to accurately define a wide range of undercuts using the two-dose method, and experiments have borne this claim out. The samples used to collect data were silicon wafers with a 100 nm layer of SiO_2. The 250 nm PMGI support layer was applied by spin coating and baked at 265 °C for 5 min, followed by the 50–100 nm 950K-PMMA imaging layer, which was baked at 180 °C for 10 min. The samples were exposed in a Raith 150 SEBL system with an electron energy of 30 keV; the lines were exposed at a dose of 400 μC/cm^2 and the adjacent undercut regions were exposed at a dose of 100 μC/cm^2. The PMMA was developed in a 3:1 isopropanol: methylisobutylketone (IPA:MIBK) solution for 180 s, and the PMGI was devel-

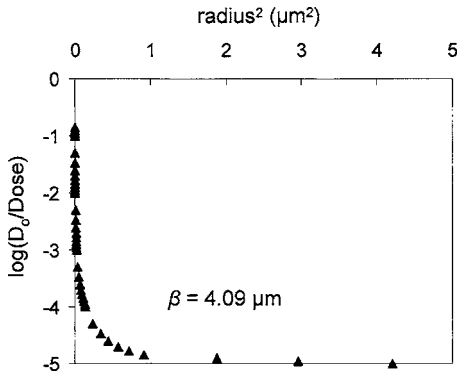

FIG. 4. Experimentally measured point-spread function for 30 keV electron exposure of PMGI, taken using single-point exposures at many doses and measuring the radii of the developed features. The backscattering coefficient extracted from this data closely matches the Monte Carlo results in Table I.

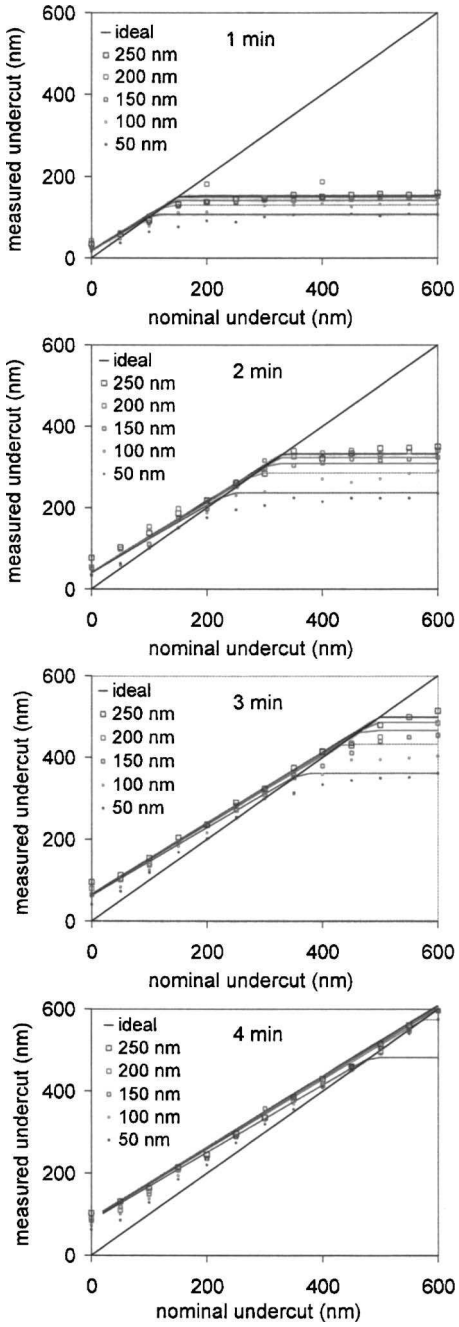

FIG. 5. Nominal vs measured undercuts for various linewidths at 1, 2, 3, and 4 min development times. At 4 min the undercut shows nearly linear behavior, but at shorter times a saturation effect is observed. This saturation effect can be accounted for by modeling the development process (solid lines).

oped in a 60% solution of CD-26 developer for 1–4 min. The resulting structures were cross sectioned and measured using a scanning electron microscope (SEM) to determine the extent of the undercuts. As Fig. 5 shows, if a sufficiently long PMGI development time was used, the experimental results closely matched the ones predicted by the model.

When the development time was reduced, a noticeable "saturation effect" was observed in the data, with undercuts that never exceeded a certain width regardless of their nominal value. This effect was more pronounced at shorter development times, and the maximum achievable undercut was proportional to the linewidth of the PMMA features. Nothing in the exposure model accounts for this behavior, suggesting that the development process may be introducing another limiting factor.

IV. DEVELOPMENT MODEL

The saturation behavior in Fig. 5 can be explained with some additional modeling of the development process. The reduction in development rate for deeper undercuts and the fact that the highest achievable undercut increased with the linewidth suggested that narrow openings in the PMMA may restrict the developer's access to the PMGI support layer. In order to quantify this behavior, a model combining mass-transfer and reaction kinetics was used to examine the development process.

Both the reaction rate and diffusion rate of the developer were taken into account in the model, in order to determine the effect of each process on the development rate. By measuring the temperature dependence of the development process, it was determined that the development reaction is a standard first-order reaction. In addition, it was assumed that the diffusion of developer through the PMMA/PMGI bilayer could be described by ordinary diffusion in a stationary medium. Operating under these assumptions allows the problem to be expressed as an equivalent electrical circuit, with the developer concentration corresponding to the voltage, developer flux corresponding to the current, and the different inhibitors of the development reaction (diffusion through the bilayer and rate of reaction) corresponding to resistors (Fig. 6). The diffusion "resistances" can be expressed as $R_D = L/DA$, where L is the length of the channel, A is the cross-sectional area, and D is the diffusivity of the developer. The resistance due to the reaction rate can be written as $R_R = 1/k_1 A$, where k_1 is the reaction rate and A is the cross-sectional area of the reaction interface. This equivalent model allows Ohm's law to be used to derive the following expression for the rate of undercut:

$$\frac{dL}{dt} = \frac{v}{1 + vAR_{\text{tot}}/\gamma C_\infty}, \tag{2}$$

where L is the undercut length, A is the cross-sectional area of the channel under the PMMA, C_∞ is the bulk developer concentration just above the PMMA layer, γ is a coefficient relating the flux of developer at the reaction site to the rate of undercut, t is the development time, v is the reaction-limited development velocity, which can be determined experimentally from the development rate of PMGI when no imaging layer is present (as in the contrast measurements in Fig. 3), and R_{tot} is the sum of all three diffusion resistors in Fig. 6. The coefficient γ is not known and the values for C_∞ and D are difficult to measure accurately, but since they always appear as a product in the equation they were treated as a single free parameter when fitting the equation to experimental data.

Using this single fit parameter, the mass-transfer model can be used to simulate undercut behavior that closely

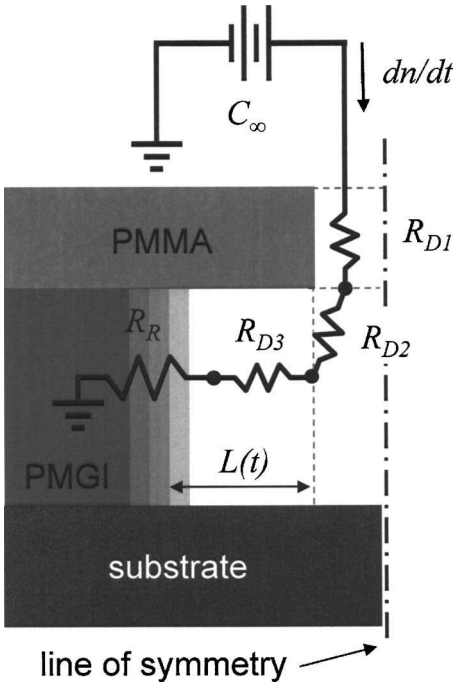

FIG. 6. Schematic diagram of the circuit used to model the development of a PMMA/PMGI bilayer. The reaction rate at the development interface and diffusion through each section (the PMMA feature, the "corner," and the undercut in the PMGI layer) can be represented by resistances, the reactant flux by a current, and the bulk developer concentration by a voltage.

matches the experimental data at all development times. The model is plotted alongside the experimental data as solid lines in Fig. 5. As in the data, the undercut shows nearly linear behavior at long development times, but when the development time is reduced a clear saturation effect is observed as the developer is forced to travel through an increasingly long undercut channel to reach the reaction site. This increases the diffusion resistance (R_{tot}) in Eq. (2) and causes the development process to undergo transition from reaction rate limited to diffusion rate limited. In the diffusion-limited regime the developer is unable to reach the reaction site efficiently, resulting in a reduced undercut rate and a maximum undercut value that is independent of the defined undercut. As expected, this saturation occurs at smaller undercut values for narrow linewidths, since the developer encounters a higher diffusion resistance when traveling through narrow openings in the imaging layer. The model also predicts the nonzero y intercepts seen in the data in Fig. 5; when the nominal undercut is very small, the developer quickly reaches the edge of the exposed PMGI and attacks the unexposed material beyond the defined undercut region, resulting in a larger-than-expected undercut.

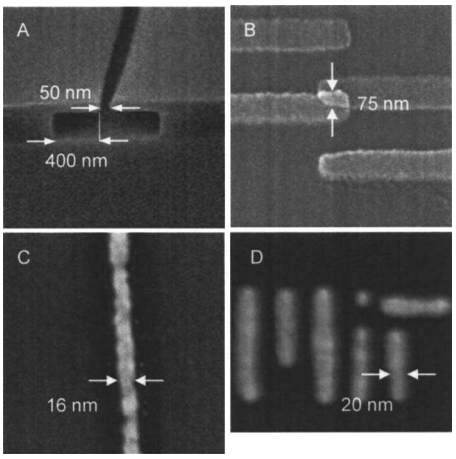

FIG. 7. (A) Scanning electron micrograph (SEM) cross-section of a 50-nm-wide line undercut by 400 nm. (B) Josephson junction with ~0.01 μm^2 area fabricated using the PMMA/PMGI process. (C) 16-nm-wide, 20-nm-thick Ti–Au line, the highest-resolution result achieved with the process to date. The PMMA imaging layer was developed with 3:1 IPA:MIBK at 0 °C here (D) 150-nm-high MIT logo fabricated in 15-nm-thick Ti–Au with linewidths on the order of 20 nm, proving that it is possible to form multiple arbitrary features in a single suspended imaging layer without the resist collapsing. The imaging layer was developed with pure IPA at 0 °C in this case.

V. CONCLUSION

By using a PMMA/PMGI resist bilayer and lithographically defined undercuts, we have demonstrated a robust, controllable process for creating high-resolution undercut structures. The exploitation of the previously undocumented high electron sensitivity of PMGI has allowed us to substantially improve on the robustness of earlier PMGI-based processes while retaining their high resolution. Through extensive modeling and experimentation, the process has been fully characterized, allowing the process parameters for any arbitrary linewidth/undercut combination to be easily determined. This allows the repeatable fabrication of lines as narrow as 20 nm with undercuts limited only by the mechanical strength of the free-standing imaging layer (Fig. 7). The process has been used to fabricate Josephson junctions with sub-0.01-μm^2 areas, and its high resolution and robustness should allow the future fabrication of many other interesting nanoscale devices and circuits as well.

[1]G. J. Dolan, Appl. Phys. Lett. **31**, 337 (1977).
[2]H. Scherer, A. B. Zorin, and J. Niemeyer, J. Appl. Phys. **97**, 54501 (2005).
[3]D. Berman, Ph.D Thesis, Massachusetts Institute of Technology, 1998.
[4]Y. Chen, K. Peng, and Z. Cui, Microelectron. Eng. **73–74**, 278 (2004).
[5]P. Hovington, D. Drouin, and R. Gauvin, Scanning **19**, 1 (1997).
[6]R. J. Hawryluk, J. Vac. Sci. Technol. **19**, 1 (1981).
[7]E. H. Anderson, D. L. Olynick, W. Chao, and B. Harteneck, J. Vac. Sci. Technol. B **19**, 2504 (2001).